PAPER

Detection and investigation of chirping Alfvén eigenmodes with heavy ion beam probe in the TJ-II stellarator

To cite this article: A.V. Melnikov *et al* 2018 *Nucl. Fusion* **58** 082019

IOP Publishing | International Atomic Energy Agency Nuclear Fusion

Nucl. Fusion **58** (2018) 082019 (8pp) https://doi.org/10.1088/1741-4326/aabcf8

Detection and investigation of chirping Alfvén eigenmodes with heavy ion beam probe in the TJ-II stellarator

A.V. Melnikov[1,2], E. Ascasibar[3], A. Cappa[3], F. Castejón[3], L.G. Eliseev[1], C. Hidalgo[3], P.O. Khabanov[1,4], N.K. Kharchev[1], A.S. Kozachek[5], L.I. Krupnik[5], M. Liniers[3], S.E. Lysenko[1], J.L. de Pablos[3], S.E. Sharapov[6], M.V. Ufimtsev[7], V.N. Zenin[1,4] and TJ-II Team[3]

[1] National Research Centre 'Kurchatov Institute', 123182, Moscow, Russian Federation
[2] National Research Nuclear University 'MEPhI', 115409, Moscow, Russian Federation
[3] Fusion National Laboratory, CIEMAT, 28040, Madrid, Spain
[4] Moscow Institute of Physics and Technology, 141700, Dolgoprudny, Russian Federation
[5] Institute of Plasma Physics, NSC KIPT, 310108, Kharkov, Ukraine
[6] CCFE, Culham Science Centre, Oxfordshire OX14 3DB, United Kingdom of Great Britain and Northern Ireland
[7] Department of Computational Mathematics and Cybernetics, Moscow State University, 119991, Moscow, Russian Federation

E-mail: melnikov_07@yahoo.com

Received 4 December 2017, revised 26 March 2018
Accepted for publication 10 April 2018
Published 29 June 2018

Abstract

Alfvén eigenmodes were studied in the low magnetic shear flexible heliac TJ-II NBI-heated plasmas by heavy ion beam probe (HIBP), which is capable to measure simultaneously the oscillations of the plasma electric potential, density and poloidal magnetic field in the bulk plasmas. The L-mode hydrogen plasma was investigated at various magnetic configurations with rotational transform $\iota(a)/2\pi \sim 1.5$–1.6. Co-, counter- and balanced beam injection were explored. The present study was focused on the high-frequency chirping modes with $250\,\text{kHz} < f_{AE} < 350\,\text{kHz}$ at the low-density $\overline{n_e} = (0.5\text{–}0.7) \times 10^{19}\,\text{m}^{-3}$ NBI-heated plasmas without auxiliary ECRH. Here we report the observation of the various types of chirping modes, differing by frequency, radial location, amplitude and shape of the frequency dependence on time (burst pattern). Remarkably, the same mode may evolve, changing its burst pattern in the same frequency range in the single discharge. The radial scan of the HIBP sample volume indicates the radial evolution of the potential and density perturbation during the single frequency burst of the chirping mode. The individual burst of the chirping-up mode can propagate outward with volume-averaged radial velocity $\approx$70 m s^{-1}. The frequency raise during the burst is in line with Alfvén frequency dependence on density, which decreases over the propagation area.

Keywords: Alfvén eigenmodes, chirping, TJ-II stellarator

(Some figures may appear in colour only in the online journal)

1. Introduction

Alfvén eigenmodes (AEs) induced by fusion α-particles and fast ions or electrons created by auxiliary heating are capable to cause losses of the fast ions in magnetic fusion devices and in a future reactor [1]. So, investigations of the AEs properties is one of the most reactor-relevant studies in the operating magnetic fusion devices, both tokamaks and stellarators, equipped by neutral beam injection (NBI), ion cyclotron resonance and electron cyclotron resonance

heating (ECRH) [2–4]. AE modes have two main forms: steady frequency mode and chirping mode. The steady frequency mode has typically a quasi-monochromatic character with a frequency, gradually evolving in time with the evolution of mean plasma parameters, like density and current. The chirping mode presents a sequence of separated individual bursts with fast frequency change in each burst, which happens at the constant values of mean plasma parameters. Both steady frequency and chirping AEs were observed in tokamaks and in stellarators [5, 6]. Typically, chirping modes have higher frequencies than steady modes, but both may exist at the same range [7].

It is believed that chirping modes may affect the fast ions in different way than more conventional steady frequency AE (convective versus diffusive transport). Chirping modes may lead to undesirable oscillations of plasma column with frequency of chirping mode [8]. Estimations have shown that unless in ITER the diffusive losses of fusion α-particles will be on the low level (~5%), the change of losses character from diffusive to convective ones due to bursts of chirping modes may strongly increase the peak power of losses and exceed the tolerable level. In contrast, measurements of fast neutral flux in TJ-II have shown that the fast ion confinement is better in regimes with chirping and mitigated AEs than in regimes with steady AEs [9].

It was found that auxiliary ECRH causes the chirping mode generation in the NBI heated plasma [10–12]. In the low-density plasmas heated by NBI and ECRH in the low magnetic shear TJ-II stellarator [13], AEs exist in the form of the chirping mode [11–15], while in the case of NBI heating only and higher densities, AEs with a steady frequency were mostly observed [16]. The most pronounced steady modes were identified as helicity induced Alfvén eigenmodes (HAEs) and global Alfvén eigenmodes (GAEs) [17, 18]. Transitions between chirping and steady AEs were reported earlier for low-density plasmas ($0.5 < \overline{n_e} < 1.5 \times 10^{19}$ m^{-3}) heated by NBI and ECRH, and these transitions were found to depend on ECRH power, plasma density and the radial location of ECRH power deposition [11].

Remarkably, another type of the plasma eigenfrequency oscillations, geodesic acoustic mode (GAM), has been also observed in the steady frequency [19] and chirping [20] mode form. For turbulence-induced GAM, the steady frequency form is typical [21], while for the fast particle induced mode, called e-GAM, both the steady [22] and the chirping modes may take place [20]. So, the study of the chirping mode properties may shed the light to the basic properties of magnetic plasma oscillations [23]. It was shown recently that the magnetic configuration has an essential effect on the frequency of the steady AEs [24] and the transition from chirping to steady modes and vice versa [7, 15].

The aim of the present study is to investigate the properties of the chirping modes in NBI plasmas in the TJ-II stellarator and to identify—if the radial location of the chirping mode is permanent. The paper presents the results of the AEs studies with heavy ion beam probe (HIBP) measurements [25, 26] supported by the AE monitoring with magnetic (Mirnov) probes (MPs) [27].

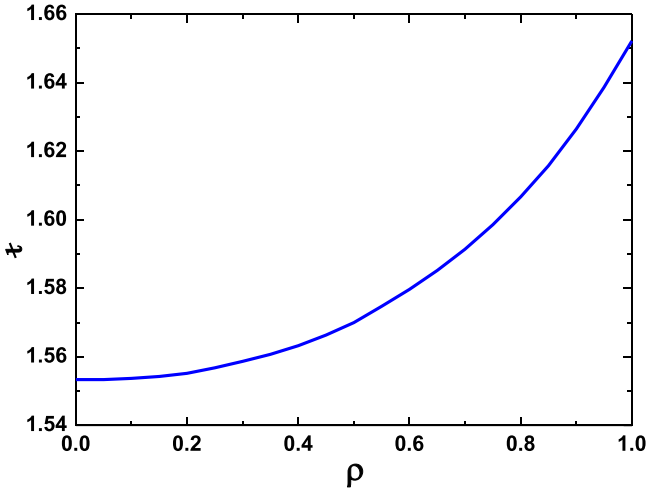

Figure 1. Vacuum rotational transform $_{vac}$ profile in the standard configuration 100_44_64 of TJ-II.

The paper is organized as follows. Section 2 describes the experimental setup. New observations of the potential/density/B_{pol} oscillations associated to AEs are presented in section 3. The radial propagation of the chirping mode is addressed in section 4. The results are discussed in section 5 and summarized in section 6.

2. Experimental setup

TJ-II is a four-period flexible heliac with low magnetic shear, and $B_0 = 0.95$ T, $R_0 = 1.5$ m, and $\langle a \rangle = 0.22$ m. Most of the experiments were performed in the standard magnetic configuration denoted 100_44_64. The numbers in this label refer to the currents in the magnetic field coils, I_{CC}_I_{HX}_I_{VF} (see figure 1 in [24]) with vacuum rotational transform $\iota_{vac} = \iota/2\pi$ increasing from $\iota_{vac}(0) = 1.55$ to $\iota_{vac}(a) = 1.65$. Here I_{CC} is a current in the Circular Coil, I_{HX} in the Helical Coil and I_{VF} in the Vertical Field Coil in kA/10. The ι_{vac} profile is shown in figure 1.

The studies were performed in Hydrogen plasmas, which were formed and heated using one or two tangential neutral beam injectors (NBI). One of them (co-injector) has beam energy $E_{NBI} = 32$ keV and deposited power $P_{NBI} \sim 0.6$ MW. It is directed along the toroidal magnetic field B_0. Another one is directed oppositely (counter-injector) and it has beam energy $E_{NBI} = 29$ keV and deposited power $P_{NBI} \sim 0.45$ MW. The beams have sub-Alfvénic velocity $V_{NBI} \sim 2.5 \times 10^6$ m s^{-1}, and $V_{NBI} \geqslant V_A/3$, where V_A is Alfvén velocity.

A typical discharge scenario is presented in figure 2(*a*). We see that in the considered L-mode discharges the line-averaged plasma density was kept at an almost constant relatively low level $\overline{n_e} \sim 0.6 \times 10^{19}$ m^{-3}, while the central electron temperature was around 300 eV. Figure 2(*b*) shows the plasma density and temperature profiles against ρ, which is the magnetic surface flux label normalized to the radius of last closed magnetic surface. It is assumed that $\rho < 0$ at the high field side (HFS), and $\rho > 0$ at the low field side (LFS) of the plasma column. The low-density ($0.4 \leqslant \overline{n_e} \leqslant 0.7 \times 10^{19}$ m^{-3}) plasmas under studies are characterized by a broad T_e profile

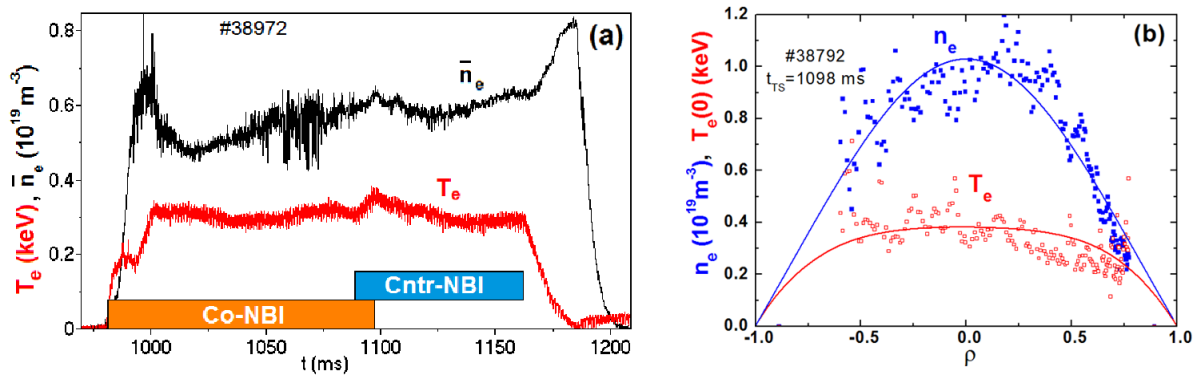

Figure 2. (*a*) The typical discharge scenario. Standard magnetic configuration 100_44_64, $P_{\text{Co-NBI}} = 0.59$ MW; $P_{\text{Cntr-NBI}} = 0.43$ MW; (*b*) the density and temperature profiles measured by Thomson scattering at $t = 1098$ ms are shown with symbols; solid lines show the fitting curves.

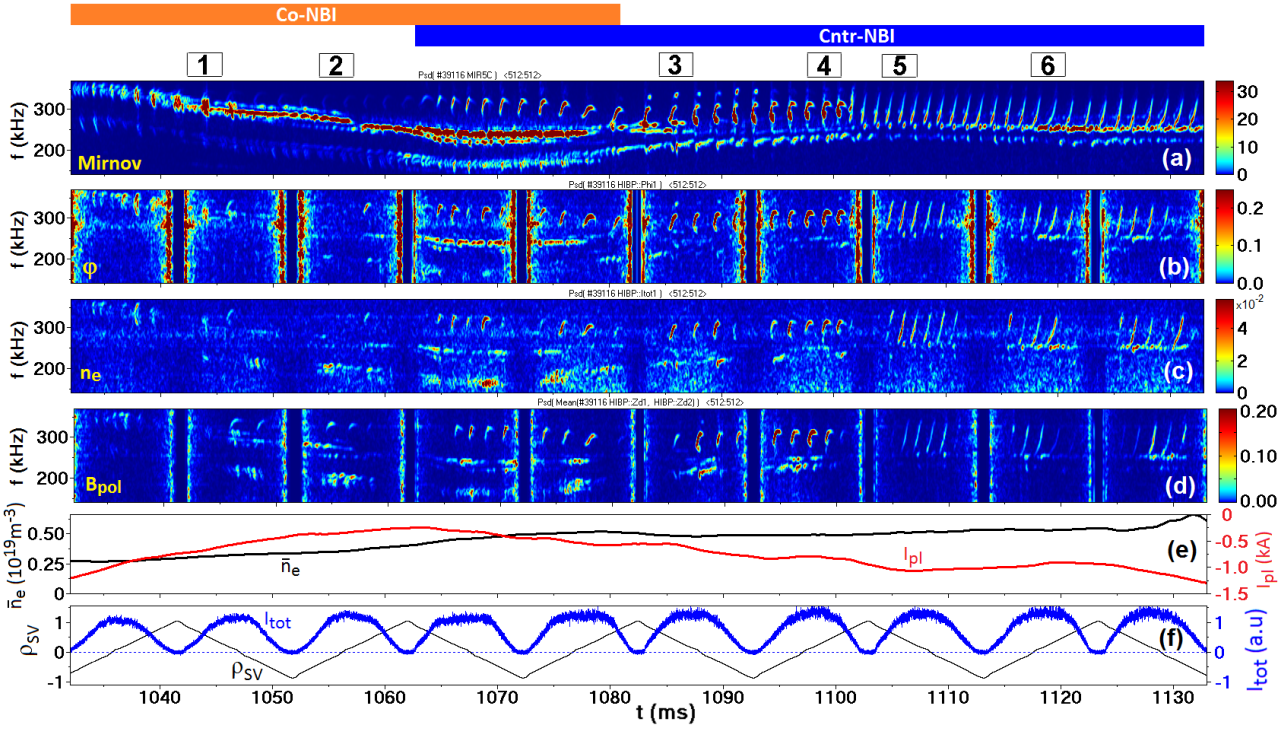

Figure 3. Chirping pattern evolution in a single shot, as observed by Mirnov probe (*a*), HIBP potential (*b*), HIBP density (*c*) and HIBP B_{pol} (*d*); (*e*) is the plasma current, measured by Rogowski coil and the mean density measured by an interferometer. HIBP operates in periodical panoramic scan mode ($-1 < \rho_{\text{SV}}(t) < 1$) shown by thin black line in (*f*); fat blue curve in (*f*) shows the sequence of density profiles, obtained in each scan. Shot #39116 with standard magnetic configuration 100_44_64, $P_{\text{Co-NBI}} = 0.58$ MW, $P_{\text{Cntr-NBI}} = 0.42$ MW. Numbers in blocks designate various patterns of chirping modes.

with $T_e(0) \sim 300-500$ eV and flat T_i profile, $T_i(0) \sim 80$ eV. At the same time, the electron density profile is generally parabolic, with rather flat core at $\rho < 0.4-0.5$ and a sharp negative slope for $\rho > 0.5$ [28].

TJ-II is equipped with a poloidal array of 24 magnetic or Mirnov probes (MPs) placed inside the vacuum vessel for measuring magnetic perturbations [27]. In addition to the MP diagnostics, we employed the Thomson scattering (TS) diagnostic, providing the density and T_e profiles once per shot, and HIBP [29, 30]. HIBP was recently used to study quasi-coherent modes [31–33] and specifically Alfvén eigenmodes [16, 17]. TJ-II is equipped by two toroidally shifted HIBP systems, which in future will allow us to explore the toroidal structure of Alfvén modes and long-range correlations [9].

HIBP allows us simultaneously measure three parameters: the electric potential and density profiles and oscillations, and the poloidal magnetic field oscillations [26]. Thus we can find the internal amplitudes of AEs. Although the HIBP diagnostics on TJ-II were described in [16, 17, 26], it is worthwhile to mention here some relevant details. HIBP operates with Cs^+ primary ions with initial energy $E_b = 125$ keV. HIBP measures the local plasma potential $\varphi_{\text{pl}}^{\text{SV}}$ in a sample volume (SV), which is proportional to the secondary beam energy

$$\varphi_{\text{pl}}^{\text{SV}} = (E_d - E_b)/e, \qquad (1)$$

where E_d is the energy of the secondary ions Cs^{++} escaping from plasma after their ionization in the SV. The local plasma

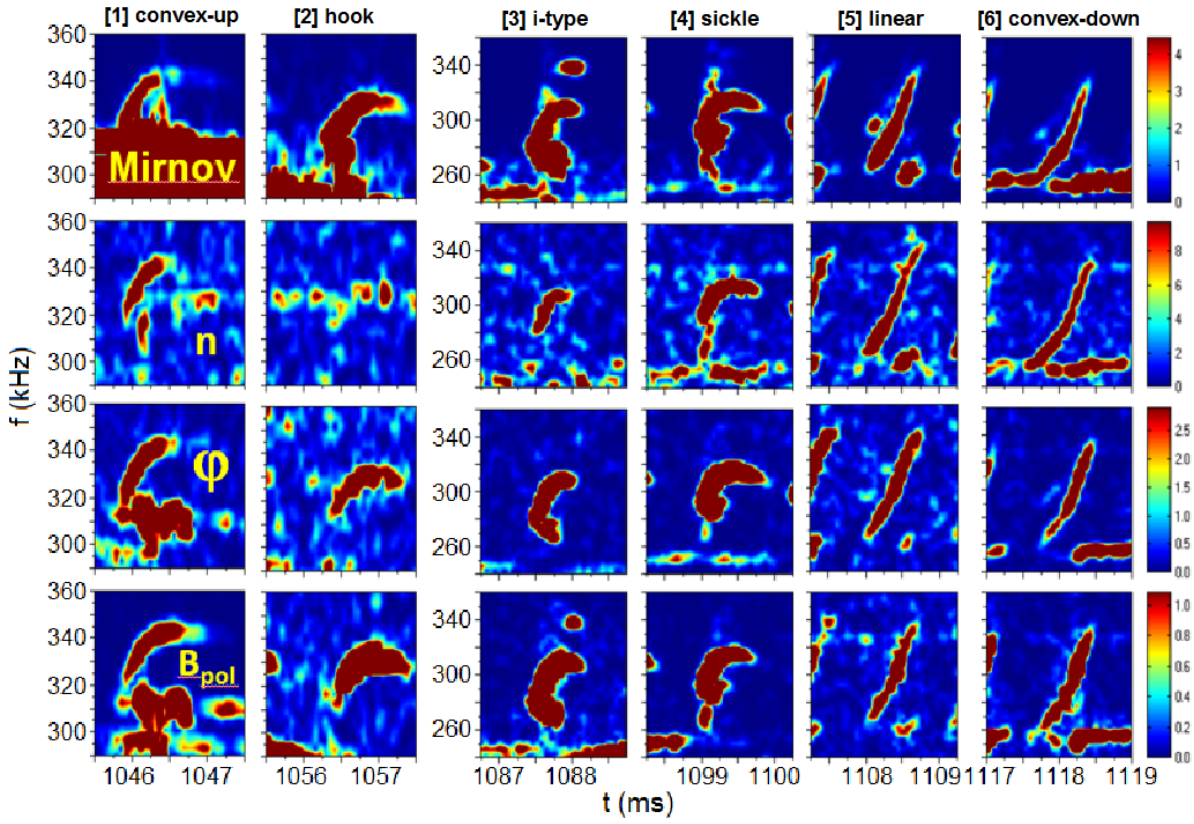

Figure 4. Multiple chirping patterns observed in a single shot presented in figure 3 with the same notations.

density n_e^{SV} in the SV is proportional to the secondary beam intensity I_{tot}

$$I_{tot}(\rho,t) = 2I_b n_e^{SV}(\rho,t)\sigma^{12}\lambda \times \exp\left(-\int_{L_1(\rho)} n_e(s)\sigma^{12}(s)\mathrm{d}s - \int_{L_2(\rho)} n_e(s)\sigma^{23}(s)\mathrm{d}s\right), \quad (2)$$

where I_b is the intensity of the primary probing beam, σ^{12} and σ^{23} are the effective cross-sections for electron impact ionization of primary and secondary ions, and λ is the length of the SV. The integrals in (2) are taken along the primary L_1 and the secondary L_2 orbits in the plasma and describe attenuation of the primary and secondary beams. The poloidal magnetic field B_{pol} creates a component of toroidal force affecting the beam orbit due to the Lorentz force.

$$m\frac{\partial \vec{V}}{\partial t} = Ze\left[\vec{V}\times\vec{B}\right]. \quad (3)$$

Here V is the probing particle velocity, m is its mass and B is the total magnetic field. Toroidal force component results in the appearance of a toroidal velocity component of the beam along the orbit. Thus, the poloidal field B_{pol} and its fluctuations may be retrieved from toroidal velocity $V_{\zeta d}$ and shift ζ_d of the probing beam in the detector using the integral relations [16]. The size of SV determines the spatial resolution of HIBP ~1 cm. In TJ-II, the SV radial position ρ_{SV} can be varied over the whole plasma column, $-1 < \rho_{SV} < 1$ [34].

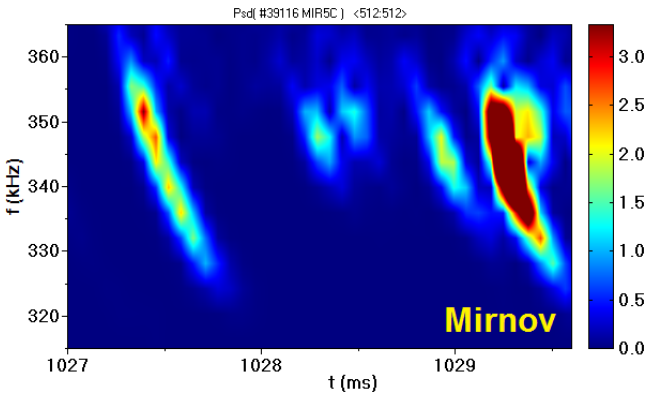

Figure 5. Chirping-down mode observation in #39116.

For the considered low-density plasmas, the mean (time-averaged) radial profile of I_{tot} has LFS-HFS symmetry. On top of that, I_{tot} increases with line-averaged density $\overline{n_e}$ up to $\overline{n_e} \leqslant 1.3\times10^{19}$ m^{-3} due to the local density raise in SV. So, the local term representing the local density perturbations in $\tilde{n}_e^{SV}$ dominates in $\tilde{I}_{tot}$ both at LFS-HFS. The same holds for ζ_d, which is indeed proportional to $\tilde{B}_{pol}$ in a SV [7]. Potential perturbation measurements are intrinsically local.

3. Chirping mode observation in the core of NBI plasma

In TJ-II, the chirping modes are typically observed in the low-density NBI discharges with or without auxiliary ECRH

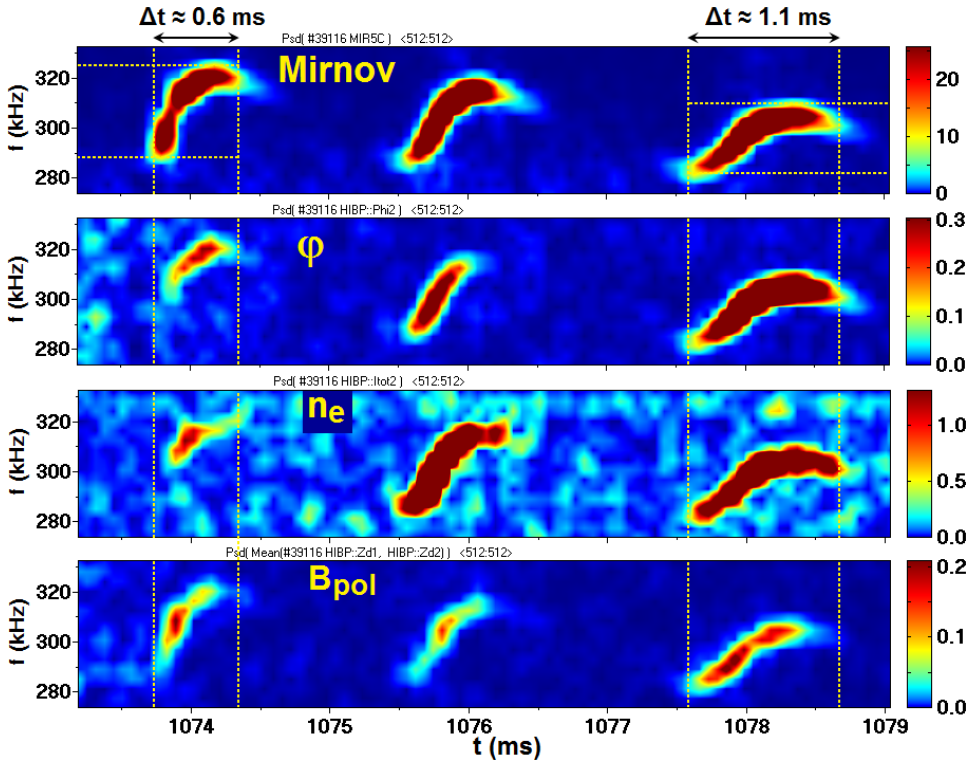

Figure 6. Time evolution of the chirping rate and burst duration for the hook pattern. Bursting ranges from 37 kHz /0.6 ms to 28 kHz/1.1 ms after three bursts. Data are taken for the shot #39116 shown in figure 3 with the same notation.

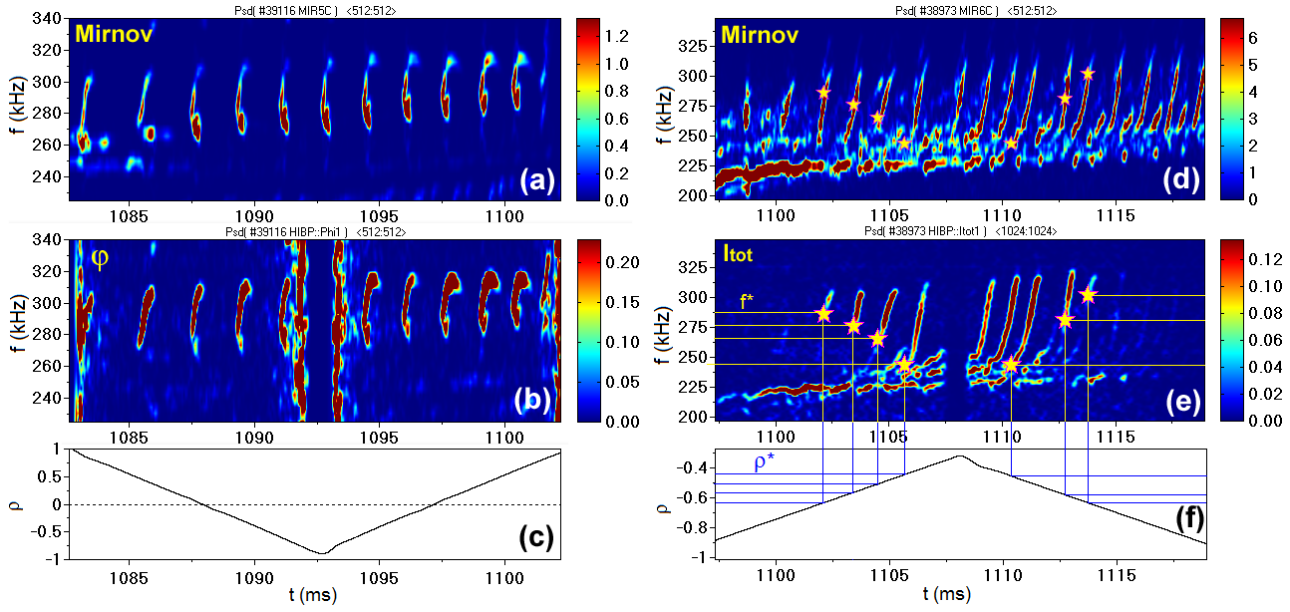

Figure 7. Observation of the unvarying hook (*a*)–(*c*) and expanding convex-down (*d*)–(*e*) patterns; (*a*) and (*d*) are Mirnov probe signals, (*b*) and (*e*) are potential (φ) and density ($I_{\rm tot}$) fluctuations. HIBP operates in the scanning mode. Stars denote the burst starting times observed by HIBP. Yellow horizontal lines shows the starting frequencies f^*, while blue lines show corresponding normalized radii ρ^*. Two similar shots # 39116 (left panel) and #38973 (right panel) were performed in configuration 100_42_64.

[7, 11, 12]. This study is dedicated to NBI-sustained plasmas. An example of AE bursts is presented in figure 3. We see the mode with a mean frequency around 300 kHz, which lasts about 100 ms. Due to the Li coating of the TJ-II vacuum vessel, the plasma density is under effective control, i.e. the low-density NBI discharges are stable and reproducible. Figure shows the very interesting and beautiful phenomenon: long-lasting chirping mode with smoothly evolving chirping pattern. The top box (*a*) presents this high-frequency chirping mode, as observed by Mirnov probe (MP). The lower boxes show this mode as observed by HIBP parameters (potential (*b*), density (*c*), and $B_{\rm pol}$ (*d*) in the panoramic scan mode of HIBP operation. Bursts with the fast frequency sweep as large 50 kHz (frequency chirping) were observed in the TJ-II plasma for the first time by

HIBP. The typical burst period in TJ-II is about 1–2 ms, while the burst 'lifetime' (time from burst appearance to the burst vanishing) is twice shorter. The HIBP radial scan lasts 10 ms, so HIBP observes 4–5 chirpings, when SV passes through the plasma diameter from LFS to HFS and back. Several different chirping patterns are marked by numbers in blocks above figure 3(*a*). One may see that each pattern is visible in the same way in all four parameters, presented in the figure.

Figure 4 shows details of patterns from figures 3(*a*)–(*c*). We can presumably distinguish six various types of chirping patterns, which differs by the shape of the temporal dependence of frequency for the monochromatic oscillations. For the first type, 'convex-up', the time trace of the mode frequency in the power spectrogram $f_{AE}(t)$ present the function with positive first derivative and negative second derivative. This is the most typical type of a chirping mode in TJ-II and also in many tokamaks and stellarators. The next one, 'hook' looks as further development of the convex-up type, when it reaches the time, where the first derivative is equal to zero and even becomes negative. Hooks are rather rarely observed on all machines. To the best of our knowledge, the other patterns are unique for AE chirping modes. The *i*-type looks like the letter '*i*' with its characteristic 'dot', located on top of the hook. The $f_{AE}(t)$ for the *i*-type presents an ambiguous function. The 'sickle' type is a kind of *i*-type, developed in time up to the reaching the negative first derivative. Similar to the *i*-type, it shows an ambiguous $f_{AE}(t)$ dependence. In contrast to *i*-type, there is no separated 'dot' on the top, but there is a kind of 'handle' linked to the bottom part of a hook. The 'linear' type presents just a line segment, while 'convex-down' has a positive second derivative. Note that for first time on TJ-II, besides chirping-up modes, we observe the chirping-down mode (figure 5) although it has been observed in many devices. Remarkably, both chirping-up and chirping-down modes appears to be in the same discharge and at the same frequency range.

Now return to other parts of figure 3. We see that the evolution of the patterns is really smooth, the wave-particle interactions process is continuous, non-interrupted. Figure 3(*e*) shows that the mean density $\overline{n_e}$ and the total plasma current I_{pl} exhibit really tiny changes, so the rotational transform ι has small changes. Figure 3(*f*) shows position of SV ρ_{SV} and the plasma density profile evolution, as measured by intensity of the secondary beam I_{tot}. We may suggest that small changes of I_{pl} and density profile cause the evolution of the chirping mode pattern. The difference in the pattern reflects the fine features of the wave-particle interactions resulting in chirping mode excitation. Tiny changes of iota and density also may cause the changes of the chirping rate and duration.

Figure 6 presents an example of such changes for the hook pattern. We see that chirping frequency range Δf decreases from 50 kHz to 30 kHz, while the burst duration increases by two times after only three bursts.

4. Radial extent of the chirping mode and radial expansion of burst

Radial scan of HIBP SV [34] is an effective tool to study AE location [16]. Fast panoramic scan presented in figure 3 allows us to observe the global picture, while slow short scan is capable to focus on details. Figure 7 demonstrates an application of this method to the hook (left panel) and convex-down (right panel) AE patterns with large frequency bursts. Top boxes (*a*) and (*d*) show the power spectrograms of the magnetic (Mirnov) perturbations, which are shown to monitor the mode behavior during the scan. Middle boxes (*b*) and (*e*) show the localized values of potential (φ) and density (I_{tot}) perturbations respectively, which depend on the SV ρ_{SV}, shown on lower boxes (*c*) and (*f*). We see that hook pattern shown in the left panel of the figure 7 are unvarying for any position of the HIBP scanning over the whole radial interval. This means that each hook occupies almost the whole plasma column from LFS to HFS. This observation is confirmed by coincidence of the starting and final frequencies for each burst measured by HIBP and Mirnov spectra.

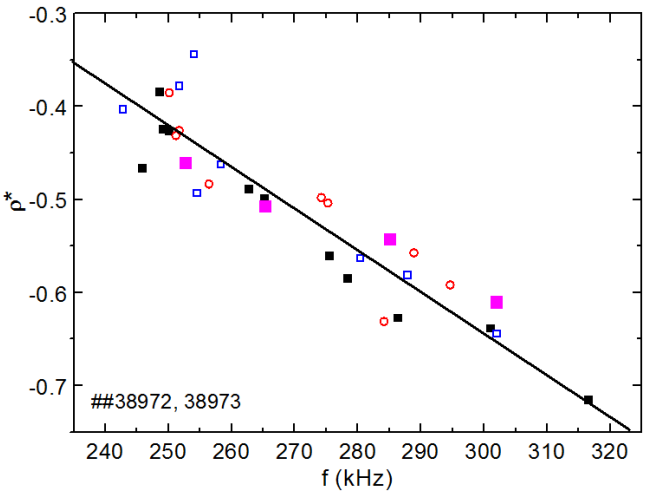

Figure 8. Dependence of the outer bound of the chirping-up AE mode (convex-up pattern) on starting frequency of the burst f^*, obtained by HIBP successive radial scans for modes on potential (open symbols) and density (closed symbols).

In contrast, the image of the convex-down pattern in HIBP signals depends on ρ_{SV}: for larger $|\rho_{SV}|$ values the burst visible by HIBP starts later in time during the burst, and, therefore, with higher frequency. In box (*e*), the time instants, at which HIBP starts detecting the burst are shown (yellow stars). The starting burst frequency is f^*, and the corresponding starting normalized radius is ρ^*. During the presented short scans in HFS ($-0.93 < \rho_{SV} < -0.3$), the HIBP measures different phases of spatial-frequency evolution of sequential bursts. Meanwhile, the global behavior of the mode does not change, as monitored by Mirnov spectrogram (*d*). To highlight the difference, we plot the stars obtained from the spectrogram of HIBP signal (*e*) to the magnetic fluctuation spectrogram (*d*). These observations are valid for both directions of ρ_{SV} evolution, no matter if ρ_{SV} increases or decreases during scan. Figure (*f*) allows us to estimate the radial range for movement the outer bound of the burst for convex-down pattern: $-0.4 < \rho^* < -0.7$.

The dependence of ρ^* on the frequency f^* is shown in figure 8. It collects the points obtained from spectrograms of plasma potential and density in several successive HIBP scans.

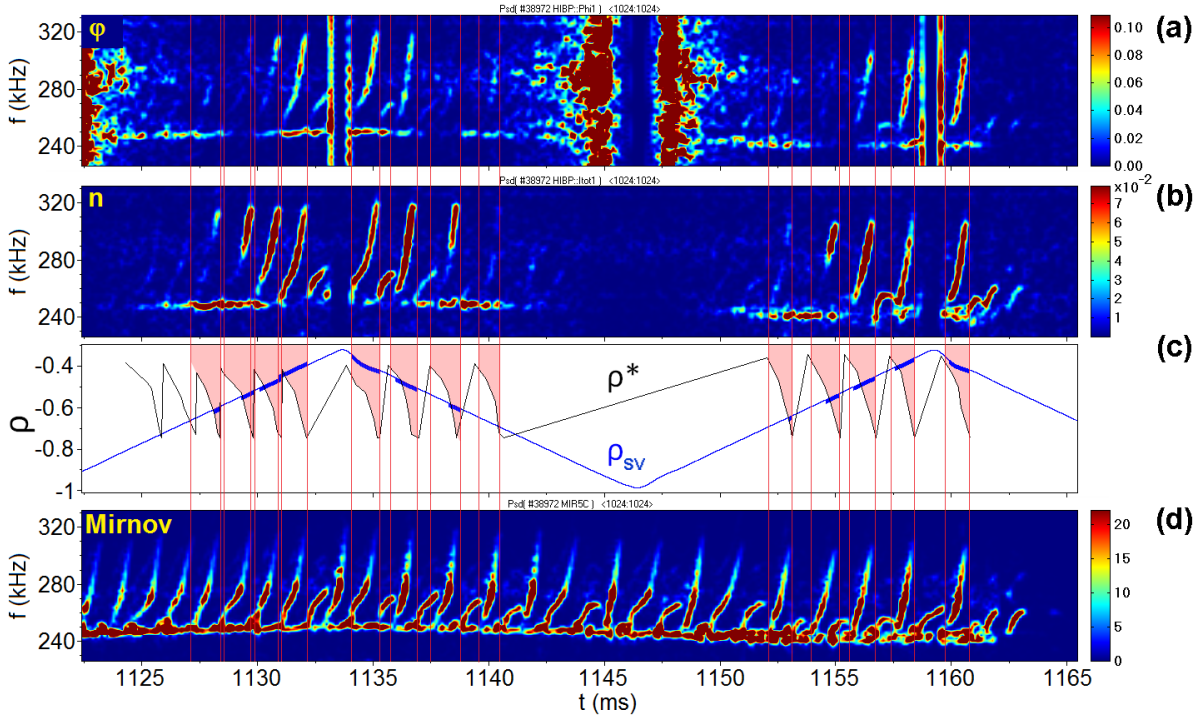

Figure 9. Chirping and HIBP scan: schematic explanation. Power spectral density evolution for HIBP potential (*a*); HIBP density (*b*); blue curve in (*c*) represents $\rho_{SV}(t)$, periodically scanned by HIBP from -1 to -0.35, Pink areas denote the time-spatial evolution of the bursts existence, which is limited by lower bound ρ^*, marked by black curve that increases in time up to the upper bound. Fat blue lines show the intersection of this area with $\rho_{SV}(t)$, representing the localization of the frequency area from starting frequency of burst f^* to the final maximum frequency of burst; (*d*) power spectrogram of Mirnov probe. Shot #38972 with standard magnetic configuration 100_44_64, convex-down-type mode evolving to linear one.

Figure 8 shows that for chirping-up AE mode (convex-down pattern), the position of outer bound ρ^* depends linearly on the low-limit chirping frequency f^*. As the value of f^* increases, $|\rho^*|$ becomes larger, indicating the outward radial expansion of the mode. At the same time, the inner bound, which corresponds to the upper frequency of each burst, remains almost unchanged, as shown in figure 7.

Figure 9 shows the spectrograms of potential (*a*) and density (*b*) with radial reconstruction of the outer bound by presenting ρ^* as a function of time for the each burst (*c*). The boxes (*a*) and (*b*) show the similarity of the typical image of the chirping mode by HIBP scan for the plasma potential and density, which is similar to figure 7. Power spectrogram of Mirnov probe, figure 9(*d*), shows that for the mode under study all bursts are same, showing frequency rise from minimum to maximum. Figure 9(*c*) presents the interpretation of the observations, shown in figures 7 and 8. Here pink color shows the area of existence of the bursts, which lies between periodically varied outer bound ρ^* and permanent inner bound. The mode under study is a chirping-up mode, so each burst starts from f^*, and reaches a constant upper frequency. This means that the burst originates some ρ^* in the core region and then, when its frequency raises, it radially expands towards the edge, while still remaining in its birth area. Near the burst origin $\rho = -0.4$, the local HIBP observes the burst during all its time duration, while near the edge it only observes the high-frequency part of the burst. The mean radial velocity of expansion may be estimated as a path from the burst origin to the maximum absolute value of ρ^*, which is $\delta\rho = 0.7–0.4 = 0.3$, as shown in figure 6, divided by the burst duration, which is $t = 1$ ms. So, the volume averaged velocity is $\langle V\rangle = \delta\rho\langle a\rangle/t = 0.3 \times 0.22$ m 10^{-3} s ≈ 70 m s^{-1}.

5. Discussion

The radial expansion of the bursts takes place at the area of the density gradient. Unless the TS data has large uncertainties for the considered low-density plasma with $\overline{n_e} \leqslant 1 \times 10^{19}$ m^{-3}, it can be estimated that the density decays in a factor of 2 from the burst origin ($\rho = -0.4$) to its outer bound ($\rho = -0.7$). According to the Alfvén law, the mode frequency for the low density at the outer bound should be in a factor of $\sqrt{2}$ higher than that at the burst origin. The ratio of the upper frequency of each burst or frequency at the outer bound (325 kHz) to the starting frequency (230 kHz) equals to 325 kHz/230 kHz $= \sqrt{2}$. So, the observation may be interpreted as follows: the mode under study originates near $\rho = 0.4$ and then expands outwards over the matter with decreasing density, encountering the frequency increase due to decay of the density in the area of expansion. The chirping modes presented here could be in principle identified as nonlinear energetic particle modes similar to those investigated in [35].

In particular, the hook mode represents a long-living nonlinear hole and clump in the fast ion distribution, for which the hook-type evolution of frequency is caused by a delicate competition between electron drag and pitch-angle diffusion effects in the collision operator. Some observed chirping

modes may be also similar to non-adiabatic EPM-like modes considered in [36], but insufficient information on the fast ion distribution function does not allow an unambiguous conclusion to be made on this.

The effect of chirping on fast ion confinement must be explored to check, if this can be beneficial.

6. Conclusions

HIBP observations show new important features of the chirping Alfvén eigenmodes in the low-density NBI discharges of TJ-II. We have found that the pattern of chirping-up mode may evolve during a single discharge with only tiny variation of plasma density and rotational transform. We have found up to six various types of the chirping pattern. During the individual frequency burst, the density and plasma potential perturbation area may expand outwards. The frequency rise is in line with the density decay in the area of expansion.

Acknowledgments

The work of Kurchatov team was supported by Russian Science Foundation (project 14-22-00193). The work of AVM was partly supported by the Competitiveness Programme of NRNU MEPhI.

ORCID iDs

A.V. Melnikov https://orcid.org/0000-0001-6878-7493
S.E. Lysenko https://orcid.org/0000-0003-1529-2088
S.E. Sharapov https://orcid.org/0000-0001-7006-4876

References

[1] Heidbrink W.W. 2008 *Phys. Plasmas* **15** 055501
[2] Breizman B.N. and Sharapov S.E. 2011 *Plasma Phys. Control. Fusion* **53** 054001
[3] Gorelenkov N.N., Pinches S.D. and Toi K. 2014 *Nucl. Fusion* **54** 125001
[4] Valovic M. *et al* 2000 *Nucl. Fusion* **40** 1569
[5] Melnikov A.V. *et al* 2015 *Plasma Phys. Control. Fusion* **57** 065006
[6] Markovič T. *et al* 2017 Alfvén-character oscillations in ohmic plasmas observed on the COMPASS tokamak *Proc. 44th EPS Conf. on Plasma Physics (Belfast, North. Ireland, 26–30 June 2017)* P5.140 (http://ocs.ciemat.es/EPS2017PAP/pdf/P5.140.pdf/)
[7] Melnikov A.V. *et al* 2016 *Nucl. Fusion* **56** 112019
[8] Gryaznevich M.P. *et al* 2008 *Nucl. Fusion* **48** 084003
[9] Castejón F. *et al* 2017 *Nucl. Fusion* **57** 102022
[10] Garcia-Munoz M. *et al* 2015 Impact of localized ECRH on NBI driven Alfvén eigenmodes in the ASDEX Upgrade tokamak *Proc.42nd EPS Conf. Plasma Physics (Lisbon, 22–26 June 2015)* P4.118 (http://ocs.ciemat.es/EPS2015PAP/pdf/P4.118.pdf)
[11] Nagaoka K. *et al* 2013 *Nucl. Fusion* **53** 072004
[12] Jiménez-Gómez R. *et al* 2011 *Nucl. Fusion* **51** 033001
[13] Ascasíbar E. *et al* 2002 *Plasma Phys. Control. Fusion* **44** B307
[14] Cappa A. *et al* 2014 Influence of ECR heating on NBI-driven Alfvén eigenmodes in the TJ-II stellarator *Proc. 25th IAEA Fusion Energy Conf. (St. Petersburg, Russia, 13–18 October 2014)* EX/P4-46 (www-naweb.iaea.org/napc/physics/FEC/FEC2014/fec2014-preprints/231_EXP446.pdf)
[15] Melnikov A.V. *et al* 2016 *Nucl. Fusion* **56** 076001
[16] Melnikov A.V. *et al* 2010 *Nucl. Fusion* **50** 084023
[17] Melnikov A.V. *et al* 2012 *Nucl. Fusion* **52** 123004
[18] Melnikov A.V. *et al* 2011 *Plasma Fusion Res.* **6** 2402030
[19] Melnikov A.V. *et al* 2006 *Plasma Phys. Control. Fusion* **48** S87
[20] Berk H.L. *et al* 2006 *Nucl. Fusion* **46** S888
[21] Melnikov A.V. *et al* 2017 *Nucl. Fusion* **57** 115001
[22] Castejon F. 2016 *Plasma Phys. Control. Fusion* **58** 094001
[23] Melnikov A.V. 2016 *Nat. Phys.* **12** 386
[24] Melnikov A.V. *et al* 2014 *Nucl. Fusion* **54** 123002
[25] Dnestrovskij Yu.N. *et al* 1994 *IEEE Trans. Plasma Sci.* **22** 310
[26] Melnikov A.V. *et al* 2017 *Nucl. Fusion* **57** 072004
[27] Jiménez-Gómez R. *et al* 2007 *Fusion Sci. Technol.* **51** 20
[28] Herranz J., Castejón F., Pastor I. and McKarthy K. 2003 *Fusion Eng. Des.* **65** 525
[29] Donné A.J.H. *et al* 2002 *Czech. J. Phys.* **55** 1077
[30] Bondarenko I.S. *et al* 2001 *Rev. Sci. Instrum.* **72** 583
[31] Melnikov A.V. *et al* 2011 *Nucl. Fusion* **51** 083043
[32] Fujisawa A. *et al* 2007 *Nucl. Fusion* **47** S718
[33] Melnikov A.V. *et al* 2015 *Nucl. Fusion* **55** 063001
[34] Melnikov A.V. *et al* 2007 *Fusion Sci. Technol.* **51** 31
[35] Lilley M., Breizman B.N. and Sharapov S.E. 2010 *Phys. Plasmas* **17** 092305
[36] Chen L. and Zonca F. 2016 *Rev. Mod. Phys.* **88** 015008